



Full Length Article

A machine learning model for multi-class classification of quenched and partitioned steel microstructure type by the k -nearest neighbor algorithmAshutosh Kumar Gupta ^a, Sunny Chakraborty ^b, Swarup Kumar Ghosh ^b, Subhas Ganguly ^{a,*}^a Department of Metallurgical and Materials Engineering, National Institute of Technology, Raipur 492010, India^b Department of Metallurgy and Materials Engineering, Indian Institute of Engineering Science and Technology, Shibpur, Howrah 711 103, India

ARTICLE INFO

Keywords:

Quenched and partitioned steels
Machine learning
Steel microstructure
Multiclass classification
 k -nearest neighbor classifier

ABSTRACT

The paper proposed a machine learning model for multiclass classification of quenched and partitioned (Q&P) steel microstructure type. In this work, we implemented the k -nearest neighbor (k -NN) algorithm to train the classifier. A Q&P steel microstructure-type database has been compiled from the previous research data comprising the information of 348 steel samples. The feature space was described by the steel composition, lower critical temperature (Ac_1), upper critical temperature (Ac_3), martensitic-start temperature (M_s), etc., and the Q&P heat treatment parameters. At the same time, the target or dependent variable was recorded as the microstructure type, for example, martensite-retained austenite {M, RA}, martensite-bainite-retained austenite {M, B, RA} etc. The proposed classifier could achieve an overall performance of 97.7% and 77.7%, measured as f1-Score in the training and testing dataset, respectively. The martensite-retained austenite {M, RA} type was found to be the most confusing class. The model explored the effect of compositional parameters and heat treatment variables on the evolution of microstructure. The re-engineering through model study for targeted martensite-retained austenite microstructure type has depicted a steel composition and heat treatment window, which has been validated by experimental development of steel microstructure. The optical and SEM micrographs, along with hardness, strongly corroborated the model analysis from a re-engineering perspective.

1. Introduction

Microstructure classification, which mainly deals with the identification of microstructural constituents or phases present in a micrograph, is an important research topic of the era. The subject is rapidly growing under the industry 4.0 perspective in association with the development of efficient AI and image processing technologies. In the design and development of steel, a microstructure remains an indispensable tool till now. Therefore, the microstructure of steel has been studied for quite a long time resulting an accumulation of a vast amount of steel microstructure data. As a consequence, the steel microstructure data analysis using the latest computational tool becomes the first choice of researchers [1–4]. Although the subjects are spread over for the study of the microstructure of metal and alloys [5–8] and digital metallography research is gaining significant momentum.

In this paradigm, the following works demonstrate the potential of analysis of steel microstructure databases in advanced steel design for the future generation. According to DeCost et al. [4], visual feature representation of micrographs can be used to compute microstructural

fingerprints and by comparing the histograms of visual features, a classification technique support vector machine (SVM) can automatically classify microstructures. Chowdhury et al. [9] used feature extraction and dimensionality reduction techniques to represent micrographs in form of feature vectors and classification was performed using k -nearest neighbors (k -NN), voting, support vector machine (SVM), and random forest models. The results displayed that a pre-trained neural network requires no previous knowledge for well representation of nature of shapes within the micrograph images. Gola et al. [10] developed a data mining process by using the support vector machine (SVM) as a classifier to develop a model that can distinguish between various microstructures of dual phase (DP) steels. They suggested that to improve the accuracy of the model, firstly morphological parameters of the second phase entity and substructure can be added, secondly, more data should be generated and used to improve generalization and to get statistically sufficient results. There is a complexity to relate subcategory microstructural constituents with principal structures at intragranular sites and prior austenitic grain boundary due to morphological and stereological effects. Thewlis et al. [11] formulated a

* Corresponding author.

E-mail address: sganguly.mme@nitrr.ac.in (S. Ganguly).

microstructure classification scheme by point-counting micrographs using a fixed grid covering a wide transformation temperature range. Azimi et al. [12] proposed a deep-learning framework for the classification of low-carbon steel microstructures. In this work, pixel-wise segmentation by means of a fully convolutional neural network (FCNN) was used. The accuracy of the proposed system was 93.94%. A UNet deep learning architecture was used by Shen et al. [13] to establish the correlation between electron backscattered diffraction (EBSD) input images and ground truth data for small experimental datasets. It was concluded that the presented method can quantitatively analyse DP and QP steels. Arivazhagan et al. [14] introduced a modified alternate local ternary pattern (MALTP), a novel texture descriptor for feature extraction with two-fold cross-validation. The two machine learning classification techniques namely k -nearest neighbor and support vector machine were used for classification of plain carbon steel microstructures. Kim et al. [15] proposed an unsupervised segmentation of steel microstructure employing the rule-based feature extraction process using different image filters and the Bayesian-Gaussian mixture model to automatically indicate a suitable number of classes.

In addition, the current evolution of steel research emphasizes the development of new advanced high-strength steel (AHSS); the trade-off between strength and formability remains the primary deal of the design consideration [16]. As microstructure determines the behavior and performance of AHSS steels, the design and control of the microstructure are crucial in the latest (third) generation of AHSS [17]. In this paradigm, the “Quenching and Partitioning (Q&P)” process has recently been substantiated to be a unique technological route to produce high-strength steel. In this class of steel, the microstructure is an architect with significant amounts of retained austenite and thus provides a better combination of strength and ductility. In this regard, the pioneering work of Speer et al. the concept of a novel and promising AHSS by Q&P heat treatment which attained a significantly better comprehensive property in steel [18]. Exploring the different facets of the Quenching and Partitioning heat treatment and resultant microstructure that offer improved properties of steel is a burning title in steel research of the recent time.

The analysis of steel microstructure has proven to be prospective for macrostructure databases of carbon steel, DP steels, HSLA steel, Multi-phase steel etc., to name a few [10,15,19–22]. Although QP steel is a recent development, however, the research in this field at different parts of the globe has already produced a significant volume of research information constituting the Q&P steel processing, microstructure, and properties database [18,23–28]. Nevertheless, the analysis of the microstructure database of this category of steel has not yet been conducted. Therefore, the present research is an effort to compile contemporary research on Q&P steel to create a QP microstructure database. The existence of a significant database on Q&P steel can help to gather more insights into this novel heat treatment process. In addition, the objective of the study is to explore the database using the state of the art of machine learning tools with a primary focus on modelling the type of microstructure evolution in Q&P steel through variation in heat treatment parameters. The article is organized as the Q&P steel microstructure dataset preparation, machine learning approach, model development and analysis of the model. Also, in the latter part, we have discussed the experimentally generated Q&P steel microstructure in view of the potential of the model in re-engineering.

2. Materials and methods

This research, with the modelling of the quenching and partitioning steel microstructure data in association with a few absolute in-house ground truth experimental data, leads to a twofold objective. First, the implementation of machine learning on quench and partitioned steel microstructure data has been discussed in the subsequent section of this article. The latter part is to validate the ability of the model to engineer the parameters for a given microstructure. In this perspective, a limited

amount of experiments are conducted. This section briefly describes the materials and experimental procedures for data reproducibility perspective.

The high-carbon Nb micro-alloyed steel (HC9) was identified to verify the reverse engineering capabilities of the proposed ML model. This steel was obtained as a forged bar from Tata Steel, Jamshedpur, India. The detailed chemical compositions noted from the spectroscopic analysis of the steel (HC9) are tabulated in Table 1.

The forged specimens (initial thickness of ~25 mm) were heated at 1200 °C for 1 h for complete homogenization. All these homogenized samples were immediately subjected to hot rolling operation in the austenite region with a finish rolling temperature (FRT) of 1000 °C and then air-cooled to room temperature. An optical pyrometer was used to maintain the required temperature after each rolling pass. The Ac_1 and Ac_3 temperatures were estimated following Trzaska [29] as 752 °C and 798 °C, respectively. The M_s temperature was estimated as 222 °C from the Andrews empirical formula [29]. Fig. 1 shows the various aspect of Q&P heat treatment of the HC9 steel. The sample was austenitized at 900 °C. The rate of austenitization was kept at 10°C/min. The first sample was subjected to one-step Q&P at 200 °C, while the other sample was subjected to Q&P heat treatment at 180°C. After Q&P heat treatment, both samples were consequently air-cooled to room temperature.

Since the microstructural investigation was the primary requirement for validating the model prediction, the hot rolled, air-cooled followed by quenching and partitioned specimens were therefore subjected to standard metallographic sample preparation methods and subsequently etched with 2% nital solution. The microstructures of all the processed specimens were obtained under an optical microscope (Carl Zeiss, Axiovert 40 Mat) and scanning electron microscope (Hitachi, S-3400N) operating at 15–20 kV accelerating voltage. For support to the microstructural constituent variation conformity against a reference, hardness values were obtained in the Rockwell hardness tester. Fifteen to twenty measurements on each sample were taken to calculate the average hardness value.

3. The machine learning approach

In this article, we proposed a machine learning implementation for a classification model of microstructure type of quenching and partitioning steel. Therefore, the framework of the machine learning approach implemented in this work is comprehensively described in this section.

3.1. Quenched and partitioned steel microstructure data

A machine learning task essentially starts with the data only. So, preparing a comprehensive dataset of quench and partitioned steel microstructure was the initial challenge in this exercise. To create a suitable dataset, extensive compositional information and the processing details, such as critical transformation temperatures and heat treatment parameters for Q&P steels and microstructural along with labelling information, were compiled from about 107 articles considering approximately 400 microstructures of Q&P steels covering about last 20 years of reported research (refer [supplementary material](#)).

It was subjected to manual investigation for inconsistency and ambiguity, which eventually yielded a dataset of size 348 × 16 comprising compositional and heat treatment parameters. An initial significance analysis suggests the drop of a few compositional parameters such as S (wt. %), P (wt. %) etc. and heat treatment time parameters from the dataset. Also, the presence of microalloying elements such as wt.% of Niobium (Nb), Vanadium (V), and Titanium (Ti) is noted as very

Table 1
Chemical composition of the investigated steel (wt. %).

C	Mn	Si	Nb	S	P	Fe
0.68	1.72	2.20	0.036	0.008	0.012	Balance

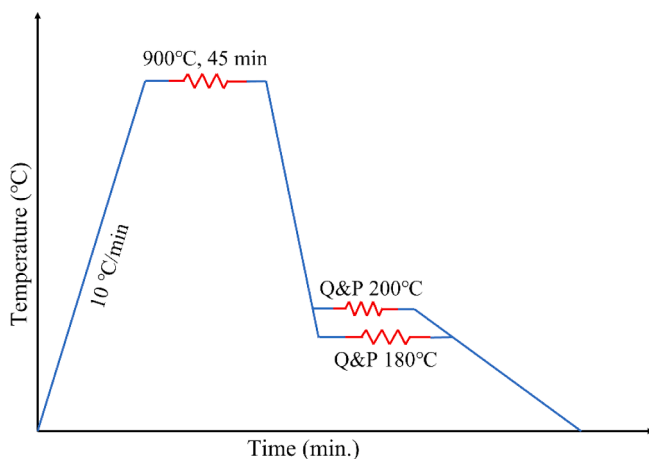


Fig. 1. Schematic illustrations of steps in Q&P heat treatment of high carbon Nb micro alloyed (HC9) steel used in the present study.

inconsistent in the dataset, which restricts them from considering each element as an individual feature. However, to avoid the loss of information in the dataset due to the importance of the microalloying effect on the microstructure of steel, they are not dropped from the dataset. It was decided to derive a new feature as a total microalloying element (TMAE), which refers to the sum of wt.% of Niobium (Nb), Vanadium (V), and Titanium (Ti). Eventually, we obtained a dataset of size 348×9 covering the feature vector C (wt.%), Si (wt.%), Mn (wt.%), TMAE (wt. %), A_1 ($^{\circ}$ C), A_3 ($^{\circ}$ C), M_s ($^{\circ}$ C), QT ($^{\circ}$ C), PT ($^{\circ}$ C). QT and PT represent the Quenching Temperature and Partitioning Temperature, respectively. A comprehensive statistical description of the dataset is tabulated in

Table 2.

The collected microstructure corresponded to the 348×9 recorded feature matrix stated above. It was investigated to categorically label different microstructure types using the expert knowledge and the reported information, which is referred to as microstructural type in this article hereafter. It was observed that there are mainly six types of microstructures exist in the dataset, which are labelled as {M, B, RA}, {M, F, B, RA}, {M, F, RA}, {M, F, RA, C}, {M, RA}, and {M, RA, C}. **Table 3** briefly describes the microstructure type with numerical coding for computational easiness. The data suggests that it is a single-label multiclass classification problem.

3.2. The model selection

Once the problem statement and the data are in hand, the very next challenge in the machine learning exercise is to assume a suitable model to train. The quenched and partitioned steel microstructure data, as stated above, depicted that it is a multiclass classification problem, and the data size is not significantly large. In such a machine learning problem, k -NN or k -nearest neighbor is contextually a good choice. Its primary advantage over the other counter-algorithms is that k -NN is simple and beneficial in the case of multiclass classification of the data [30,31].

k -NN is a nonparametric machine learning algorithm under the supervised learning category. In other words, k -NN does not imply any assumption on the data under study. The basic underlying theory of this algorithm is that closely related things are located nearby. The mathematical concept of this algorithm is very simple. One needs to know three crucial things, k , the number of nearest neighbors, distance metrics (Euclidean distance, Manhattan distance) and the majority vote on which the k -NN classifier algorithm is founded. Although the techniques

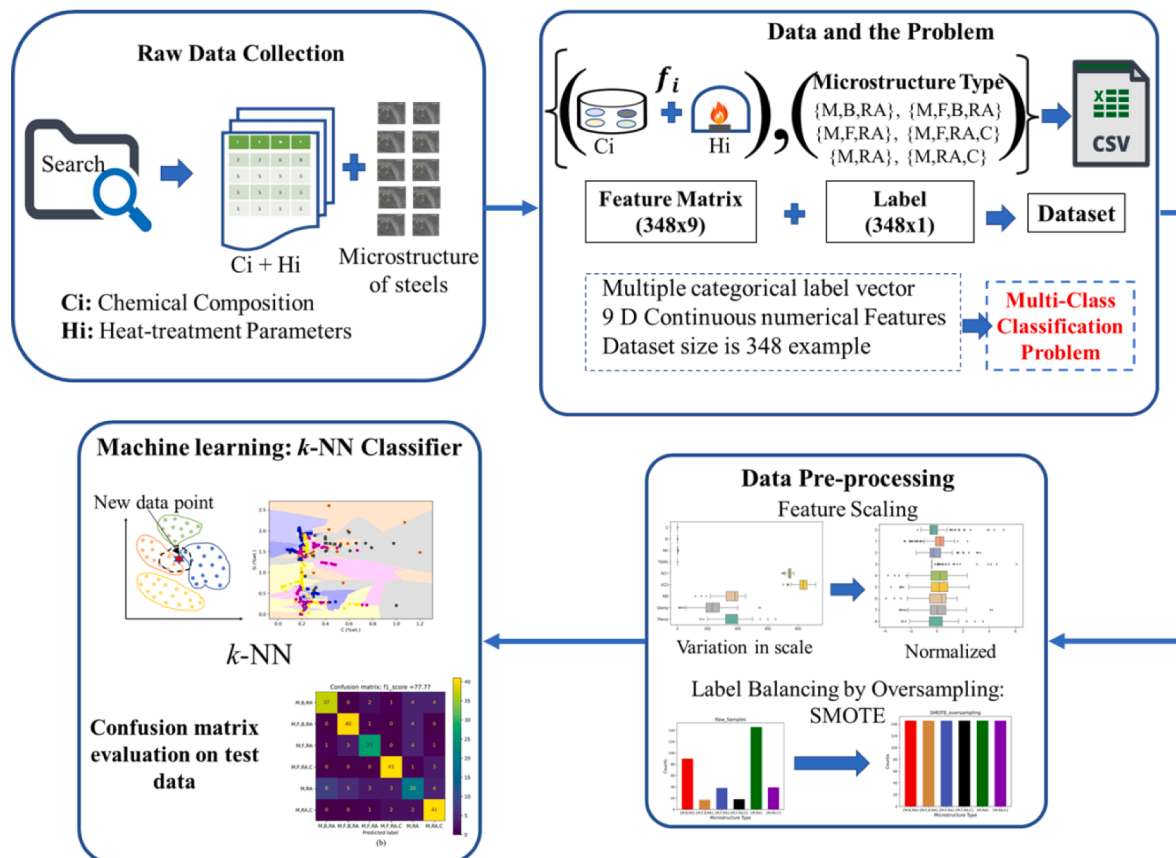


Fig. 2. Schematic description of the computational methodology for quenching and partitioning steel microstructure type classification model development using k -NN.

Table 2
Features used in microstructure type data.

	Features	Description	Max	Min	Mean	SD
Inputs (Features)	C	wt. % of carbon	1.20	0.03	0.29	0.18
	Si	wt. % of silicon	2.60	0.00	1.35	0.54
	Mn	wt. % of manganese	6.00	0.24	2.11	1.18
	TMAE	wt. % of microalloying element	0.30	0.00	0.02	0.05
	Ac ₁	Lower critical temperature (°C)	772.50	693.87	742.42	13.01
	Ac ₃	Upper critical temperature (°C)	916.44	703.28	829.26	35.76
	M _s	Martensite starts temperature (°C)	453.60	120.00	359.01	61.23
	QT	Quenching Temperature (°C)	550.00	10.00	228.50	76.29
	PT	Partitioning Temperature (°C)	650.00	150.00	367.09	80.29

Table 3
Description of Q&P-steel microstructure type, which acted as the label or response variable in the present machine learning problem.

Microstructure Type	Description	Numerical Code for the class of microstructure type
M, B, RA	Martensite, bainite and retained austenite microstructure	0
M, F, B, RA	Martensite, ferrite, bainite and retained austenite microstructure	1
M, F, RA	Martensite, ferrite and retained austenite microstructure	2
M, F, RA, C	Martensite, ferrite, retained austenite with carbide microstructure	3
M, RA	Martensite and retained austenite microstructure	4
M, RA, C	Martensite and retained austenite with carbide microstructure	5

are commonly used for classification problems, they can be used for regression problems as well. In that case, the prediction is made by averaging of nearest neighbor instead of majority voting. Unlike other ML algorithms, it does not train the dataset instantly but rather stores them in memory during the training phase, which triggers certain realization when classification is performed on a new data point. The working principle of the *k*-NN algorithm can be described as follows:

- 1. Selection of *k*, i.e., number of neighbors:** The selection of *k*- is the most crucial in building a *k*-NN. There is no straightforward strategy or best choice for *k*. Trial and error methods are used to find the best *k* values. Even values are usually not used in classification problems to avoid tiebreaker situations in majority voting. Small values yield an unstable model. Larger values are good, however, and lead to some difficulties. The choice of *k*-value as 5 is very common and works well for a wide variety of data.
- 2. Computation of the distance for nearest neighbors:** computation of distances of a given data point and the point in the dataset is a concern in *k*-NN modelling. The computational complexity depends on the number of data points in the training dataset (*N*) and the dimension of each data point (*D*, length of feature vector). Brute force, *k*-D Tree, and ball tree are popular algorithms used to reduce the computational complexity based on the data, i.e., *N* and *D* values.
- 3. Consider the *k* nearest neighbors based on the computed distance metrics:** From the obtained distance metrics as resulted from step 2, first *k*-numbers of nearest neighbors are indexed, and their classes are recorded.
- 4. Counting of the number of data points in each class from these *k* neighbors:** The frequency of each class out of the *k*- nearest neighbors is computed at this step.
- 5. The class allocation for the new data points:** It is done by majority voting strategy; the class corresponding to the highest number of neighbors is allocated for the new data points.

6. The predictive model is ready for testing and evaluation: Predictions can be made on the test data to evaluate the performance of the model.

The details of the evolution of the *k*-NN model for the present classification of the microstructure type of Q&P-steel are explained in the latter section of this article.

3.3. Model evaluation

The proposed model for the present problem is a multiclass classification model. Therefore, the confusion matrix, which depicts the error in the model, is used for the evaluation of the model performance. A confusion matrix is an *N* × *N* matrix where each entry *e_{ij}* is the number of cases predicted as the *j*th class, which is actually *i*th class. From a confusion matrix of four important numbers. These are, the cases are positive and predicted as positive, True Positive (TP), cases are negative and predicted as negative, True Negative (TN), the case is positive but predicted negative, False Negative (FN) and the case are negative but predicted positive, False Positive (FP). In comparison, TP defines the number of occasions that our actual positive cases match the anticipated positive cases. The number of times our model incorrectly predicts negative values as positives refer to as the FP. The number of instances when our actual negative cases match our anticipated negative cases is known as TN, and the number of times our model incorrectly predicts negative cases as positives denote FN. These numbers are calculated for each class one at a time, and that class is treated as *Positive* while the rest except that class are considered as *Negative*, for instance. Using these four numbers, the following matrices are computed.

The ability to correctly predict a class out of the total number of cases predicted as that class is referred to as precision which accounted for type I error. For each class, it is defined as the ratio of TP to the sum of a TP and FP. Precision can also be termed as the accuracy of positive predictions.

$$\text{Precision} = \frac{\text{TP}}{\text{TP} + \text{FP}} \quad (1)$$

On the other hand, the ability to correctly predict a class out of the total number of cases actually of that class is referred to as recall. For each class, it is defined as the ratio of TP to the sum of TP and FN. Recall can also be termed as a fraction of positives that are correctly identified.

$$\text{Recall} = \frac{\text{TP}}{\text{TP} + \text{FN}} \quad (2)$$

Moreover, the *f1 score* is another metric that refers to a weighted harmonic mean of precision and recalls such that the best score is 1 and the worst is zero. So, as a rule of thumb, the weighted average of the *f-score* is a more acceptable performance metric for a classifier than overall accuracy.

$$\text{F1 score} = \frac{2 \times (\text{Recall} \times \text{Precision})}{\text{Recall} + \text{Precision}} \quad (3)$$

Overall accuracy is a gross performance measure which is defined as the ratio of the sum of the correctly predicted cases out of the total

number of cases.

$$\text{accuracy} = \frac{TP + TN}{TP + FP + TN + FN} \quad (4)$$

Support is the number of actual occurrences of the class in the specified dataset. Imbalanced support in the training data may indicate structural weaknesses in the reported scores of the classifier and could indicate the need for stratified sampling or rebalancing. Support doesn't change between models but instead diagnoses the evaluation process.

In the present implementation, the f1-score was used as the performance indicator metric.

4. Model development

The proposed machine learning model development plan and methodology are summarized in Fig. 2. It comprises a few components such as raw data collection, structuring the data and problem description, data pre-processing, and, eventually, model development using an ML algorithm. A primary diagnostic of the data and structuring it to make it a component for machine learning, it evolved that the problem is a multi-class classification problem, which involves a dataset comprised of 348 examples. The feature (input variable) space is defined by a 9-

dimensional vector, while the label vector is a multi-class categorical data as summarized in Table 2 and Table 3. Considering the dataset and nature of the multi-class complexity of the label vector k-NN classifier was found to be competent for this modelling problem. A detailed description of data pre-processing and model development overview is presented in the following subsections.

4.1. Data preprocessing

Fig. 3 shows the histogram plot for each of the features (independent) variables, which depicts the distribution pattern of the features in the compiled dataset. The histograms are a type of bar plot for numeric data that group the data into bins for a graphical representation of data distribution. The X-axis represents the values (bin ranges) of the feature, while Y-axis shows the counts of occurrence. It can be observed that the C (wt.%) varies between 0.03 and 1.2, but most of the data are centered around 0.2; for Si (wt.%), data is centered around 1.6, for Mn (wt.%) mostly data is concentrated between 1 and 3. The total microalloying elements, which include Nb, Ti and V, are mostly concentrated in around 0.05 wt%. The critical temperatures and quenching (QT) and partitioning temperatures (PT) show a good distribution over their range

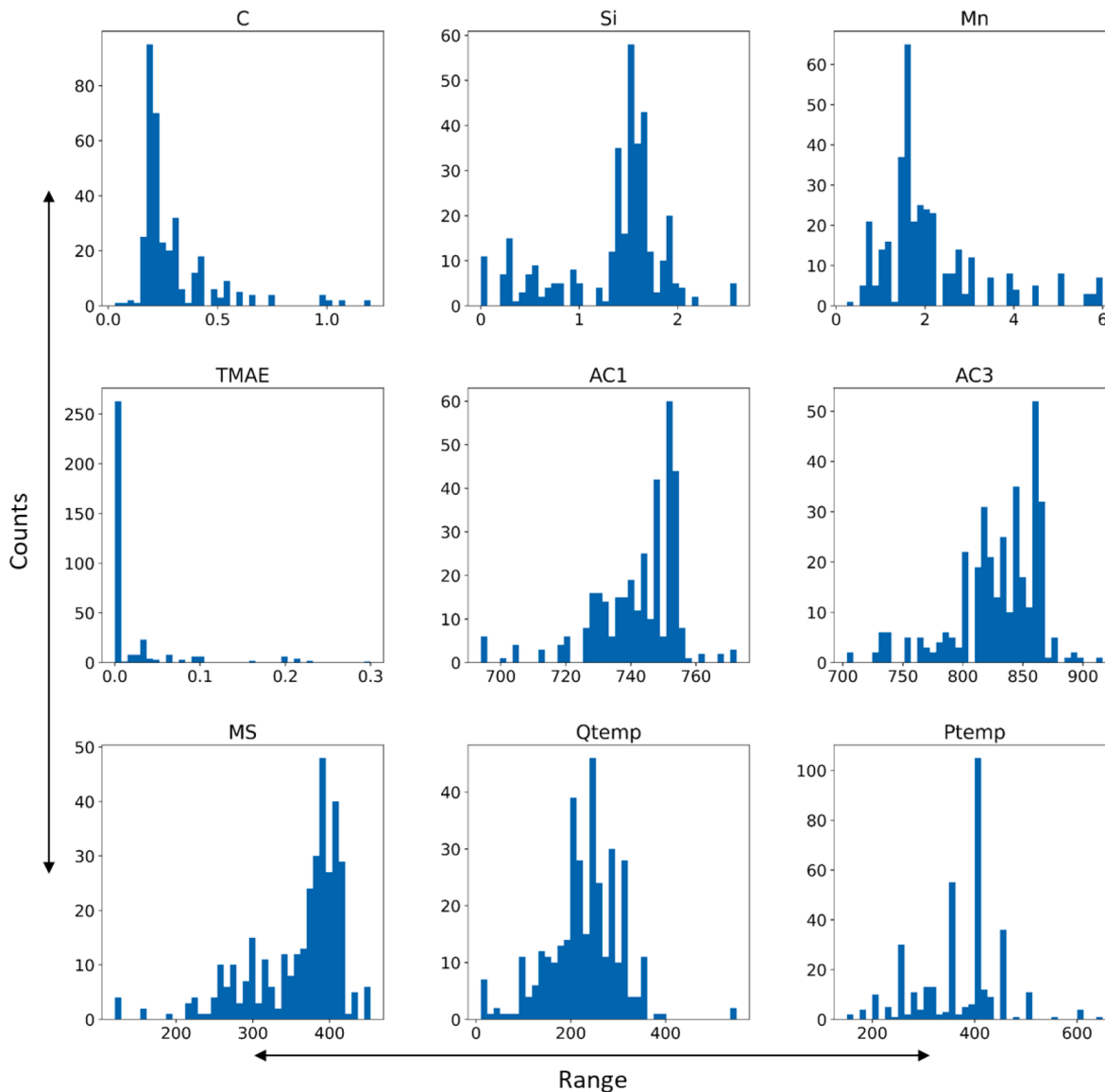


Fig. 3. Histogram plot for the features (Independent variables).

normally distributed.

It is noteworthy that all the features are continuous variables, and the numerical values vary in order from small fractions (compositional features) to a few hundred (temperature features). In such a situation, the machine learning literature recommends scaling the dataset to avoid biased learning due to significant differences in the scale across the features. Therefore, before executing ML algorithms, the collected data were standardized to zero-mean following the expression shown in Eq. (5).

$$x_i' = \frac{x_i - \mu}{\sigma} \quad (5)$$

where x_i' is the standardized feature value corresponding to x_i , μ and σ are the mean and standard deviation values of the original feature column x , respectively.

Fig. 4(a) visualizes the pairwise relationship between the variables. In comparison, the pairwise correlation is shown in Fig. 4(b). The kernel

density estimate (KDE) plot on the diagonal of Fig. 4(a) demonstrates the distribution of each variable over the frequencies of the microstructure type class. While the scatter plots on the lower triangle show the lack thereof (relationship) between the pair of features. For example, in the C (%wt.) and Si (%wt.), the scatter plot shows that they are positively correlated and depict that C (%wt.) variation in the high Si (%wt.) range tends to evolve a distinct class. Similarly, in bottom-right plot between Ptemp and Qtemp showing a linear line mark of {M, RA} category of microstructure, revealing the one-step quenching and partitioning (Ptemp = Qtemp) treatment. Fig. 4 also shows that the {M, RA} and {M, B, RA} are dominating class over other classes. This signifies the class imbalance problem in the dataset.

A further diagnostic on the label vector, it was noticed that the classes (i.e., MST) in the dataset are significantly imbalanced. The bar plot of classes shown in Fig. 5(a) represents the counts of six microstructure types that appeared in the collected dataset. The representation of steels with microstructure class {M, F, B, RA} and {M, F, RA, C}

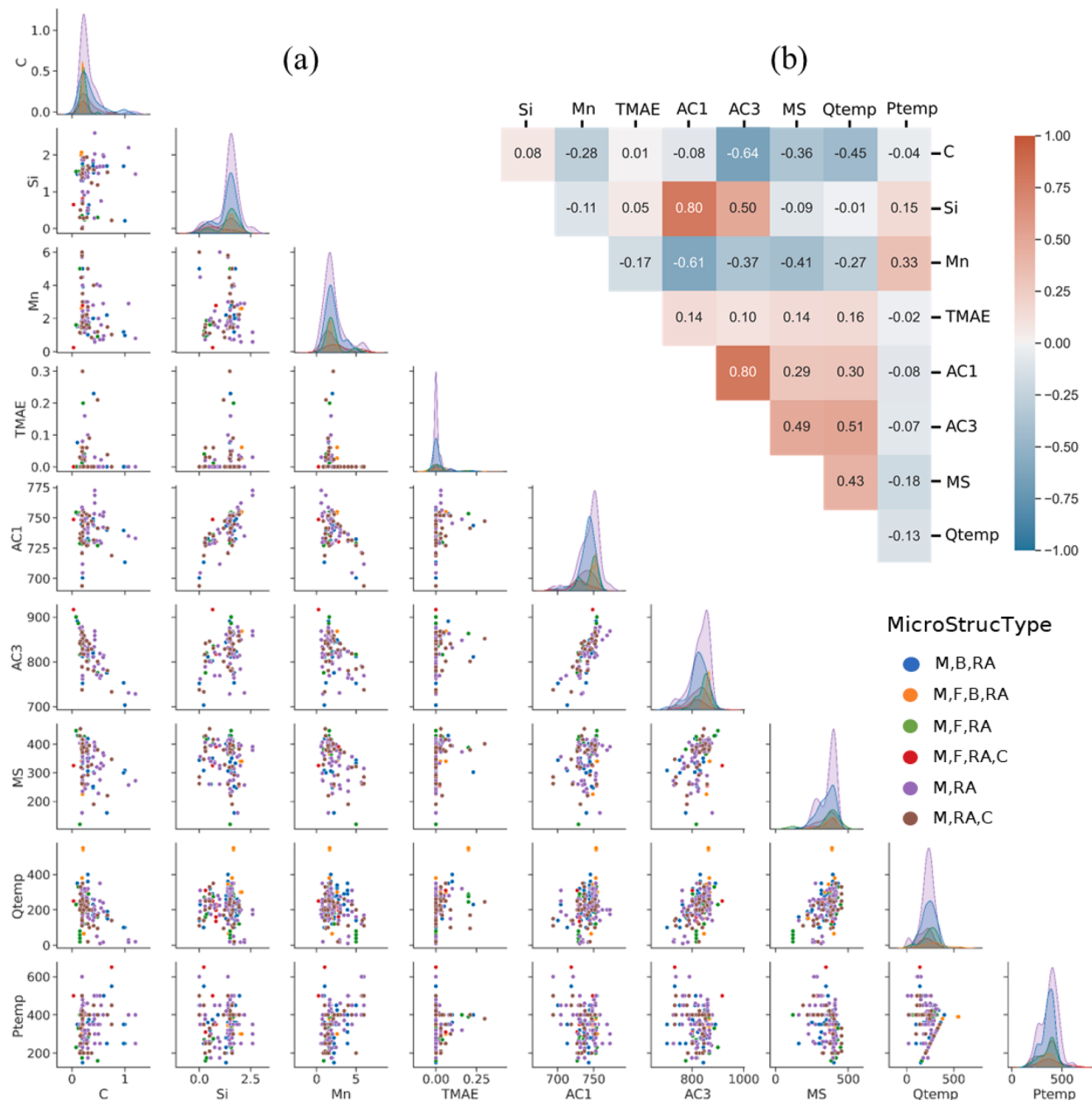


Fig. 4. (a) Pair plots of feature space to discover the relationship between the features, if any, in the dataset, (b) Heat plot (correlation) matrix of features space to discover numerical values of the correlation between the features.

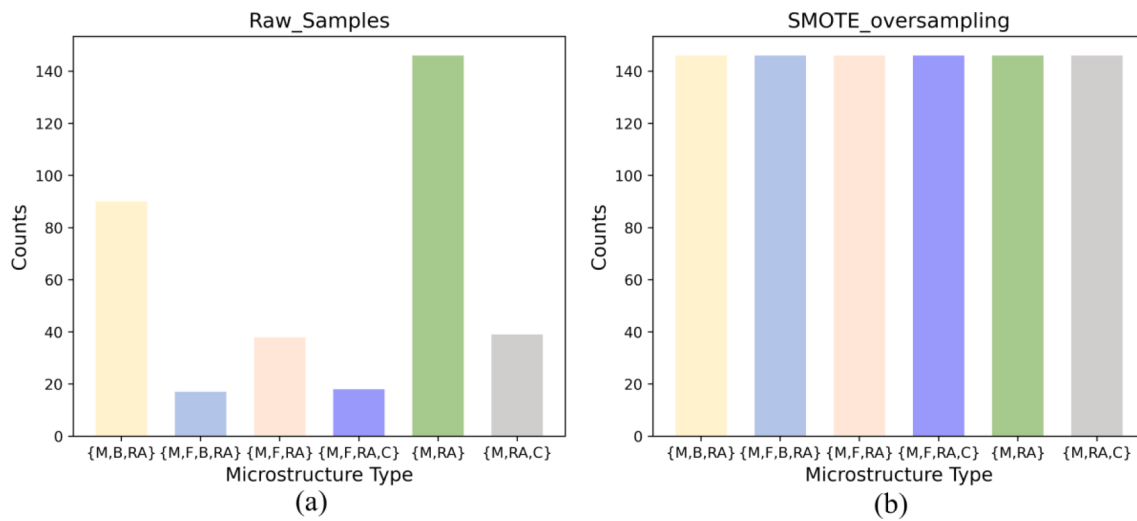


Fig. 5. Histogram of the collected data before and after class balancing by SMOTE oversampling.

are significantly low, along with the few more classes having poor representation in the data. Considering this anomaly in the data, we have applied the synthetic minority overbalancing technique (SMOTE) in the pre-processing stage of the model-building task.

The oversampling function has been utilized to eliminate the aforesaid misbalancing issue. In this case, SMOTE oversampling is performed to equalize the sample size. In SMOTE oversampling, each category's sample is increased to the highest frequency (counts) of the class (i.e., up to 146 in this case). The sample size of the raw (originally collected) dataset and SMOTE oversampling data are compared and shown in Fig. 5.

4.2. k-NN Classifier

As stated before, in this work, we have implemented k -nearest neighbor as the classifier for Q&P-steel microstructure data modelling. Eventually, the pre-processed Q&P-steel data was used to train the classifier. The dataset was spitted in a 70/30 ratio for training and testing purposes. A Python code using the sci-kit learn package was developed to train the k -NN classifier. Fig. 6(a) and (b) show the typical illustrative representation of the model in the %C vs %Si space and Q-temperature vs P-temperature space. Nevertheless, the actual model is in the nine-dimensional feature space. The different colour regions on the map show the microstructure type region, while colour-filled circles are training data points.

Choosing the k -value is a crucial step for training a k -NN classifier, as stated before. For this purpose, the classifier was trained with different k -value, and the model performances were evaluated with f1-Score in the test dataset to set an optimal value for k . Fig. 7 shows the performance of the classifier for a range k -value while other model parameters remain in default settings ({'algorithm': 'auto', 'leaf_size': 30, 'metric': 'minkowski', 'metric_params': None, 'n_jobs': None, 'n_neighbors': 5, 'p': 2, 'weights': 'uniform'} default parameter). It can be noted that a 5-neighbor k -NN, which is also known to be the most common k -value, was found to be the optimal value for the Q&P-steel microstructure type classification model. Moreover, the hyperparameter tuning has been performed to tune the base model with hyperparameter grid {'n_neighbors': [3,5,7,9,11,13,15], 'weights': ['uniform', 'distance'], 'algorithm': ['ball_tree', 'kd_tree', 'brute'], 'leaf_size': [15,20,25,30], 'p': [1,2]} which evolved the optimal parameter setting as 'n_neighbors': 5, 'weights': 'distance', 'leaf_size': 20, 'p': 2, and 'algorithm': ball_tree.

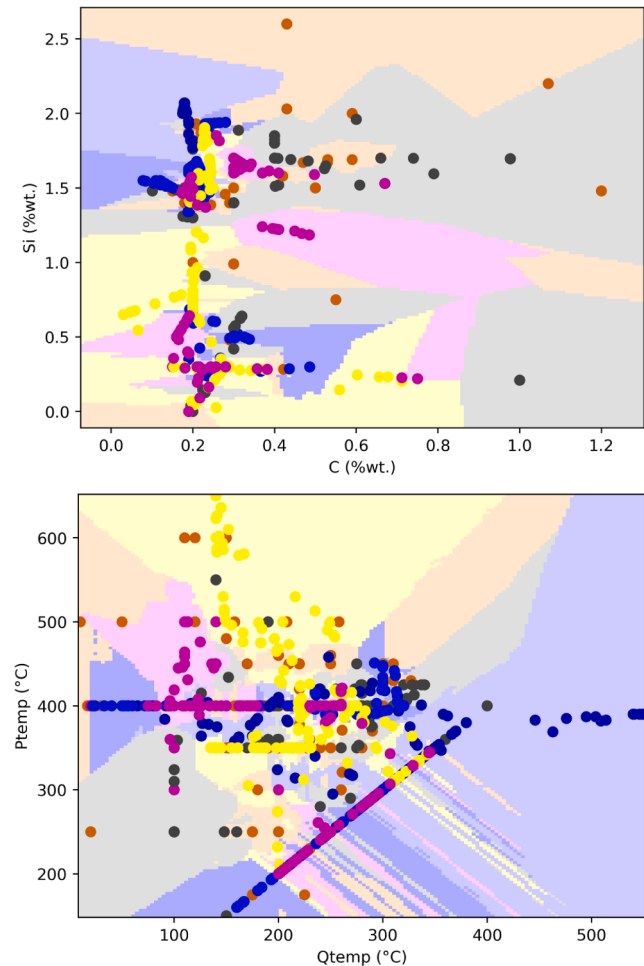


Fig. 6. Illustrative classification map of proposed k -NN model typically, in (a) C (wt. %) vs Si (wt. %) and (b) Q-temperature vs P-temperature space.

5. Results and discussion

5.1. Model evaluation

Fig. 8 shows the typical confusion matrix for multiclass classification

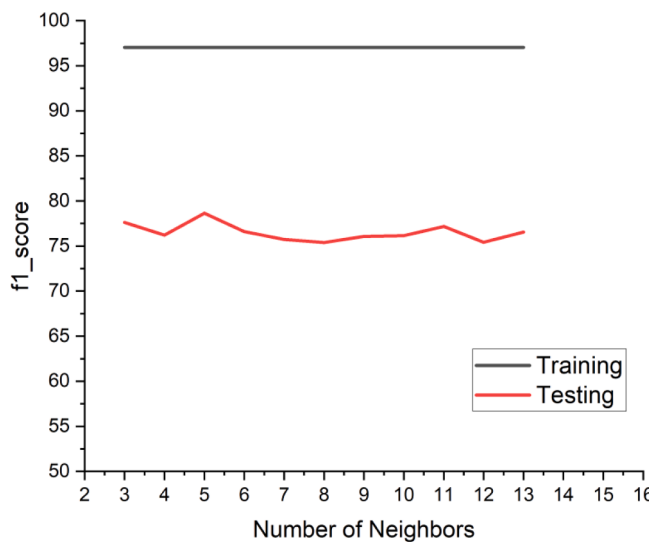


Fig. 7. Evolution of k-value for the proposed k-NN classifier by evaluation f1-score as performance metric on the training and testing dataset.

of Q&P steel microstructure type obtained from the proposed k-NN model. The confusion matrix summarizes the performance of the model on the training and test dataset. It is a potential visualizer which provides much deeper information about the type of error committed by the classifier, if any. The accuracy of the classification alone may mislead the understanding of the performance of the model if the fractions of correctly predicted observations in each class are uneven. For example, in the present exercise, the number of correctly predicted cases for the six microstructure types concerning their support in the test data set is uneven. Particularly in the case of {M, RA} seems to be unlike the other five classes. In this case, the accuracy of the models uniquely may not be the correct metric to measure the model performance. In the present context, it depicts the correctly classified and misclassified numbers for the various classes of Q&P steel microstructure, namely {M, B, RA}, {M, F, B, RA}, {M, F, RA}, {M, F, RA, C}, {M, RA}, and {M, RA, C}.

The confusion matrix grossly highlighted the overall accuracy of the classification of the Q&P steel microstructure type. The test data confusion matrix (Fig. 6,(b) right side) demonstrated the success and failure of the correct predictions for each of the microstructure types of Q&P steels. Moreover, it can be noted that the {M, RA} type

microstructure is a more confused class to be predicted and may need repeated experimental verification for certainty. Out of the 43 cases which are actually {M, RA} in the test data, the classifier correctly predicted 20 cases only. Out of the rest of the 23 cases, 8, 5, 4, 3 and 3 are confused with {M, B, RA}, {M, F, B, RA}, {M, RA, C}, {M, F, RA} and {M, F, RA, C} type of microstructure respectively. It can be attributed that achieving the pure martensite and retained austenite {M, RA} microstructure is difficult. A small fraction of the presence of one ore of micro-constituents like bainite, ferrite or carbides is highly prone to this microstructure, which seems a metallurgically obvious possibility.

The performance of the k-NN classifier precisely measured by precision, recall and f1-score for each of the microstructure types are obtained and tabulated in Table 4, usually referred to as the classification report. The overall classifier performance is depicted by the macro average of precision, recall and f1-score, which measured as 0.77, 0.78 and 0.78, respectively, on the test data comprised of 263 examples. The f1-score, which accounts for the harmonic mean of the precision and recall, was considered the performance metric of the proposed k-NN classifier in this application. All the microstructure types in the test dataset except {M, RA} show more than 0.75 precision, recall and f1-score values. However, in the case of {M, RA} class precision, recall and f1-score are shown 0.57, 0.47 and 0.51, respectively. In other words, the microstructure type {M, RA} appeared as the most confusing class for model prediction among all the microstructure types. Therefore, for the microstructure class {M, RA}, the type I error (precision) and type II error (recall) are both signs that lead to poor f1-score. So, in use of this model when prediction yield {M, RA} need cautious confirmation through real experiments. Nevertheless, the model prediction is significantly reliable for the remaining five microstructure classes.

Table 4
Classification report on the test dataset showing the model performance matrices of the proposed k-NN classifier for Q&P steel microstructure type.

	Precision	Recall	f1-score	Support
M, B, RA	0.80	0.77	0.79	48
M, F, B, RA	0.83	0.89	0.86	45
M, F, RA	0.79	0.75	0.77	36
M, F, RA, C	0.87	0.91	0.89	45
M, RA	0.57	0.47	0.51	43
M, RA, C	0.77	0.89	0.83	46
Accuracy			0.78	263
Macro avg.	0.77	0.78	0.78	263
Weighted avg.	0.78	0.78	0.78	263

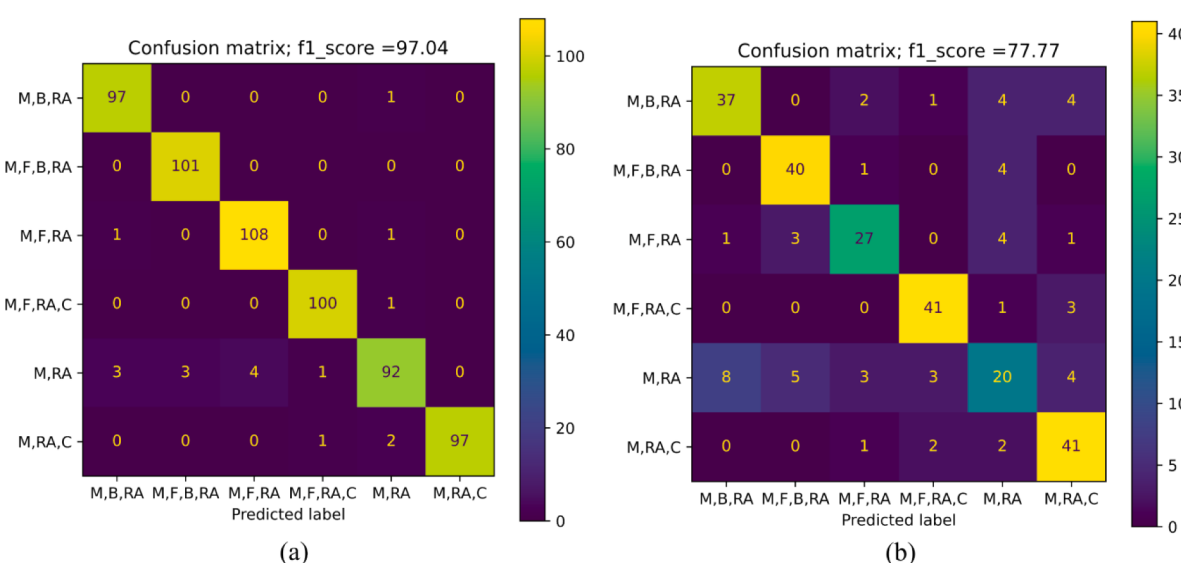


Fig. 8. Confusion matrix depicting the gross performances of the k-NN classifier on the (a) training data and (b) test data.

5.2. Model insight and re-engineering for target microstructure

Fig. 9 shows the model insights in terms of the study of compositional variables such as C (wt.%), Si (wt.%), Mn (wt.%), TMAE (wt.%); and heat treatment temperature such as Qtemp (°C) and Ptemp (°C) on the evolution of microstructure type of the steel. A synthetic dataset was produced, taking all the features with average values except the one for which the effect has been evaluated. For example, in the case of the study of effect C (wt.%), the other feature variables: Si (wt.%), Mn (wt.%), TMAE (wt.%), QT (°C) and PT (°C) were set constant at their average values, i.e., 1.35, 2.13, 0.02, 742, 829, 357, 227 and 368, respectively, while values for Ac_1 (°C), Ac_3 (°C), M_s (°C) were computed using formulas as stated before. The effect of C (wt. %) was explored by a model prediction for various values of the C in its range. Similar processes have been repeated for each of the features. **Fig. 9** is the predicted results to study the effect of each variable on the evolution of Q&P microstructure. Each subplot in **Fig. 9** depicts the predicted microstructure against the variation of individual features. The Y-axes represent the microstructure type class. It can be seen from the figures that the low carbon range favors martensite-retained austenite with ferrite, {M, F, RA} type multi-phase microstructure. To account for the effect of the silicon content of the steel on the resulting microstructure, the model insight suggests that less than 0.5%wt. Si may produce {M, B, RA} multi-phase microstructure. Nevertheless, for a wide range of Si%wt., from around 0.75 to 2.25, a high chance of formation of {M, RA} type microstructure has been found.

The subplot showing the effect of Mn is found to be interesting in Q&P steels. It divides the compositional range into two interesting parts that lead to the evolution of two different types of microstructures. The Mn up to 4 wt% is likely to produce {M, RA} type microstructure, while the Mn in the range of 4 to 6 wt% has predicted for {M, F, RA} type microstructure. These wide variations in predicted microstructure type of steel with the variation of Mn (wt.%) is interesting as the partitioning of Mn plays an important role in the competitive transformation of austenite to martensite and stabilization of austenite. Thereby, it yielded

the relative presence of martensite and retained austenite in the microstructure. The low TMAE (total micro-alloying elements) potentially changes the microstructure from {M, RA} type to {M, B, RA} type. The low quenching is seemingly responsible for {M, RA} type microstructure, and however, above 300°C can produce {M, B, RA} type microstructure. The effect of partitioning temperature is predominantly predicted for mainly two different microstructure types, that is {M, RA}, and {M, RA, C}; however, at a higher temperature, a tendency towards formation {M, B, RA} is prominent. The partitioning temperature below 200°C is responsible for the carbide-free formation of {M, RA} while between 200 and 600°C partitioning temperature predicted the presence of carbide in the microstructure.

We also conducted a computer experiment to re-engineer the steel composition and heat treatment parameters for a target microstructure type. Although, the model prediction analysis reported above has identified {M, RA} type microstructure as the most confusing class. The uncertainty associated with the prediction of this microstructure type is relatively high as compared to the other class. However, for a deeper knowledge of the classifier on the prediction behavior, the {M, RA} type microstructure was chosen as the target microstructure to re-engineer the composition and heat treatment parameter. Also, these results were implemented for real-life experiments and the development of the steel, which we reported in the subsequent section.

For this study, a dataset was generated considering five levels for each C, Si and Mn % wt. as {0.03, 0.32, 0.615, 0.91, 1.2}, {0.04, 0.68, 1.32, 1.96, 2.6} and {1.0, 1.75, 2.5, 3.25, 4}, respectively. Three distinct levels of TMAE were chosen with values as 0, 0.016 and 0.036 % wt. The data set yields a full factorial experiment combination of the compositional space. The Qtemp and Ptemp for this experiment were initially set constant at average values, i.e., 229 and 367 °C, respectively. The Ac_1 , Ac_3 and M_s have used calculated values as usual. k-NN model prediction was performed on this data set of size $5 \times 5 \times 5 \times 3$. **Fig. 10** shows the prediction of the microstructure type (refer to **Table 3** for numerical code). It is noteworthy that the microstructure class {M, RA} i.e., 4, is consistent in compositional space of C % wt. = 0.61, Si % wt. in the

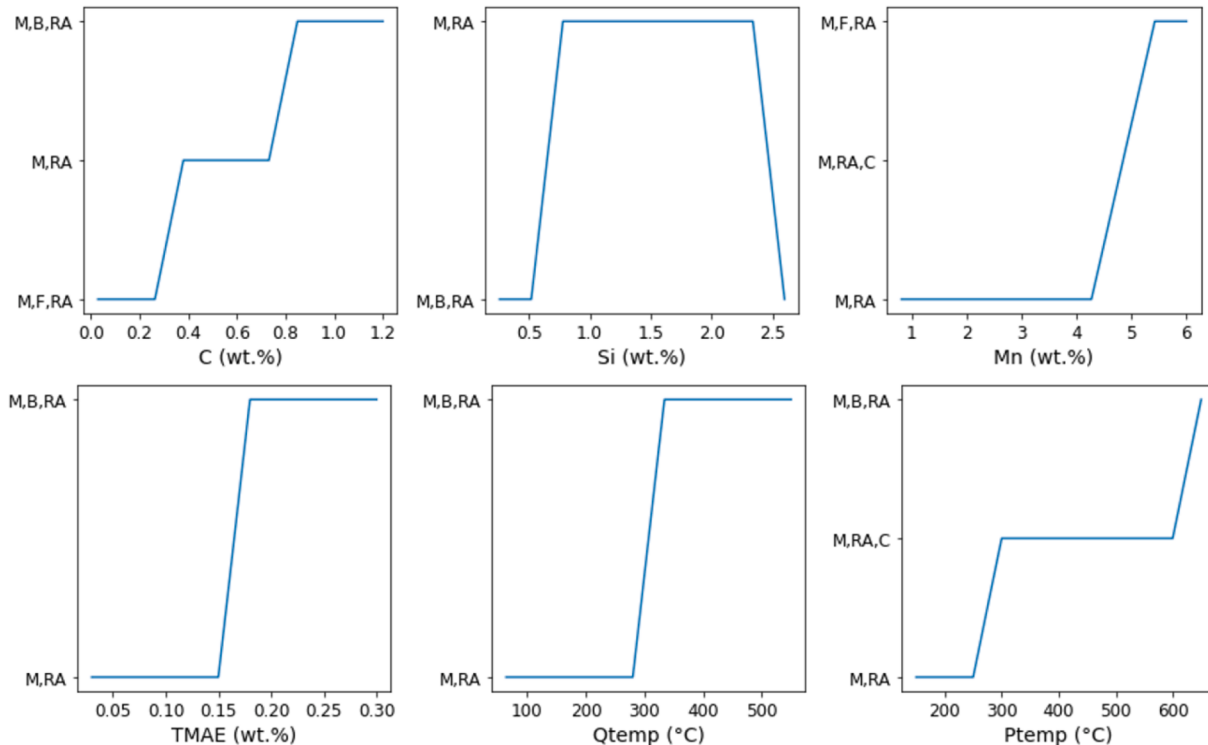


Fig. 9. The proposed k-NN classifier prediction of the effect of various composition and heat treatment parameters on the evolution of steel microstructure type. All the parameters were kept at average value except the one for which the effect was predicted.

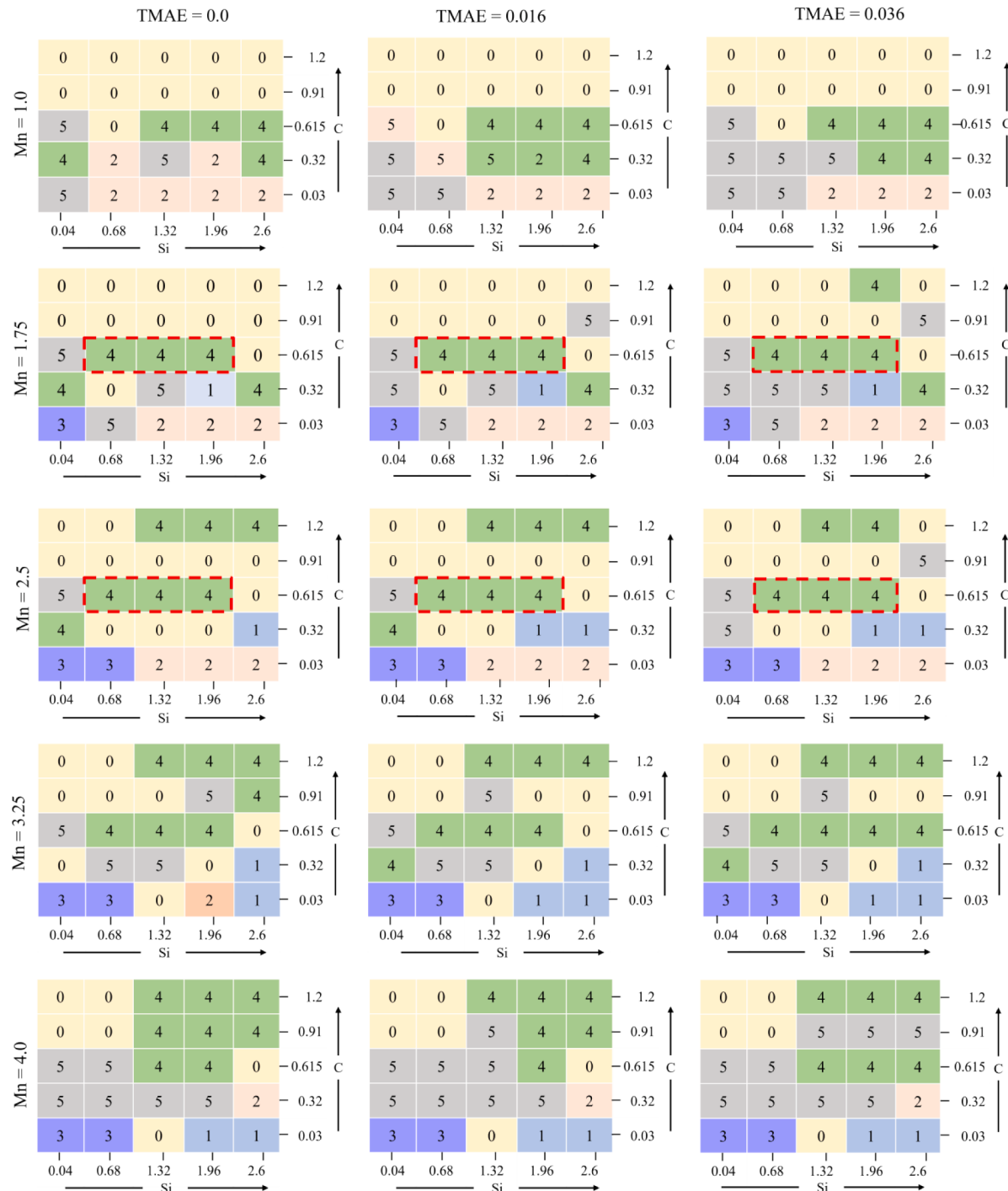


Fig. 10. Exploring the proposed k-NN classifier prediction of Q&P steel microstructure type for re-engineering the compositional feature. The numerically coded (refer to Table 3) Q&P steel microstructure type is shown as predicted by the classifier for the synthetic dataset created by C, Si and Mn and TMAE % wt. setting at different levels, as shown in the figure, while the heat treatment parameters were kept at average values (Qtemp = 230 °C and Ptemp = 250 °C).

range of 0.68 to 1.96, and Mn % wt. in almost the entire range of 1.0 to 4.0, respectively, for all three TMAE values. Considering this potential range, the composition has been proposed for target {M, RA} microstructure type as C = 0.70 % wt., Si = 1.8 % wt., and Mn = 2.0 % wt.

The proposed composition has been further investigated for consistency of prediction over heat treatment temperatures, i.e., Qtemp and Ptemp and these computer experiments have been repeated for both TMAE values of 0.016 and 0.036 %wt. Fig. 11 shows the prediction of microstructure type for heat treatment temperature variations. A potential temperature regime has been identified in the case of TMAE

content about 0.036 %wt. for {M, RA} or four microstructure type classes. However, a very narrow zone is visible in the TMAE level of 0.016 %wt.

5.3. Experimental development of Q&P steel for targeted microstructure

From the model analysis presented above in the context of re-engineering of {M, RA} type microstructure, a target composition of C = 0.65 to 0.70 % wt., Si = 0.70 to 2.0 % wt., Mn = 1.5 to 2.0 % wt. with TMAE 0.036 %wt. were decided for the real synthesis of the steel

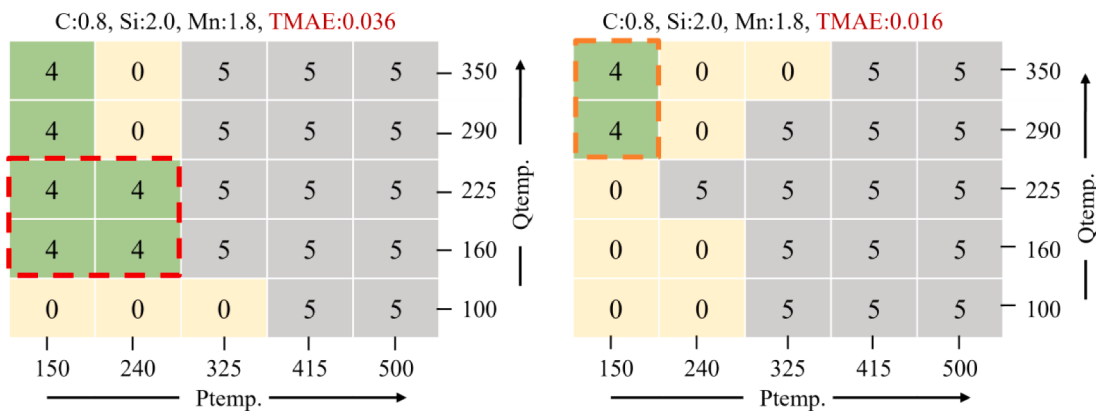


Fig. 11. The proposed k-NN classifier prediction of various Qtemp and Ptemp at different values while the chemical composition was kept constant. Exploring the proposed k-NN classifier prediction of Q&P steel microstructure type for re-engineering the heat treatment parameter such as Qtemp and Ptemp. The numerically coded (refer to Table 3) Q&P steel microstructure type is shown as predicted by the classifier for the synthetic dataset created by setting Qtemp and Ptemp at a different level, as shown in the figure, while the composition was kept constant as evolved from the analysis of the prediction shown in Fig. 10 (C = 0.8, Si = 2.0 and Mn = 1.8 and TMAE = 0.016, 0.036).

and actual lab investigation. Eventually, the laboratory-synthesized steel achieved the following compositions in wt. %: C-0.68, Mn-1.72, Si-2.20 and Nb-0.036.

Fig. 12(a) and (b) show the optical and SEM images of the steel before Q&P heat treatment. The proposed steel was hot-rolled and air-cooled with a finish rolling temperature (FRT) of 1000°C. It is noticeable that a prior austenite grain boundary (PAGB) is visible in the microstructure, which has been marked with a bright dashed line in the optical micrograph. The clear evidence of prior austenite grain boundary indicates the presence of bainite/martensite in the microstructure. The dark regions at the grain boundary, as evident in Fig. 12, are attributed to the possible presence of pearlite (P). The dark regions of pearlite are of varied thicknesses along the grain boundary. The pearlite formation can be due to the slow cooling (air-cooling) rate after hot rolling. The high hardness value of 66 HRC indicates the presence of a hard phase like martensite (M) in the microstructure, which can be attributed to the higher hardenability due to Mn, Si and Nb additions in the present high carbon (0.68 wt%) steel.

For this steel, the Ac_1 , Ac_3 , and M_s temperatures were estimated from the previous equations and came out to be 752 °C, 798 °C and 222 °C, respectively. Eventually, steel was subjected to one-step Q&P (Qtemp = Ptemp) at two different temperatures, 180 °C and 200 °C, which are expected to be lower than M_s (222 °C) and the specimens were marked with S1 and S2, respectively. The detailed description of the validation plan for the development of the steel and real experimentation to verify the proposed re-engineering obtained from the model predictions is

presented in Table 5.

Fig. 13 shows the optical and SEM micrographs of specimens S1 and S2, as detailed in Table 5, which are steel specimens after being subjected to Q&P heat treatment as stated above. The optical and SEM micrographs of the S1 steel specimen. The optical and SEM micrographs of sample S1 correspond to those subjected to one-step Q&P at 200°C. It can be observed that the microstructure mainly consists of martensite (M) and retained austenite (RA). As the QT is much lesser than the M_s , martensite formation is obvious. Here, due to Q&P, no traces of dark regions of pearlite are present in the microstructure. There is also a reduction in the hardness from 66 HRC to 64 HRC. This can be attributed to the formation of retained austenite which reduces the hardness and enhances the ductility. The retention of austenite implies more carbon is required for its stabilization, thus making the martensite more devoid of carbon. Moreover, a considerably rapid quenching rate in Q&P rules out any possibility of undesired pearlite formation. Thus, the primary constituents are martensite and retained austenite which interestingly matches with the model prediction.

The optical and SEM micrographs of specimen S2 correspond to the sample subjected to one-step Q&P at 180°C. In this case, the prior austenite grain boundary (PAGB) is occupied by the ferrite (F) phase of white contrast. The formation of ferrite is attributed to the redistribution of carbon in austenite through diffusion and austenitic regions having low carbon content transform to ferrite before quenching at 180°C [32]. The dark martensite (M) phase can be observed throughout the micrograph. No large islands of retained austenite (RA) can be observed in the

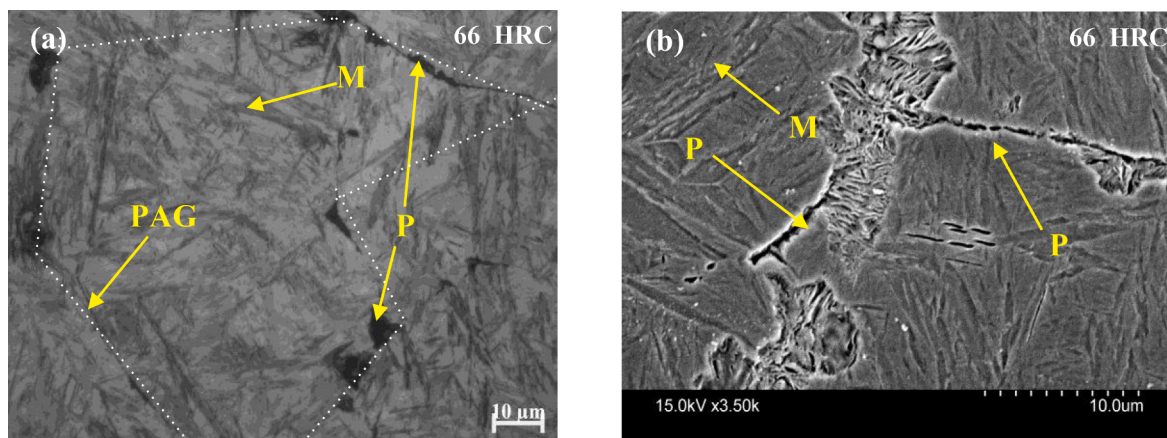


Fig. 12. (a) Optical and (b) SEM micrographs of the hot-rolled and air-cooled sample (HC9-HRAC-FRT1000).

Table 5

Description of the compositional, critical temperature and heat treatment temperature variables (features) for developing steel and real experimentation to validate re-engineering from the model prediction.

Sample IDs	Feature vectors								
	C	Si	Mn	TMAE	Ac ₁	Ac ₃	M _s	Qtemp	Ptemp
S1	0.68	2.20	1.72	0.036	752	798	222	200	200
S2	0.68	2.20	1.72	0.036	752	798	222	180	180

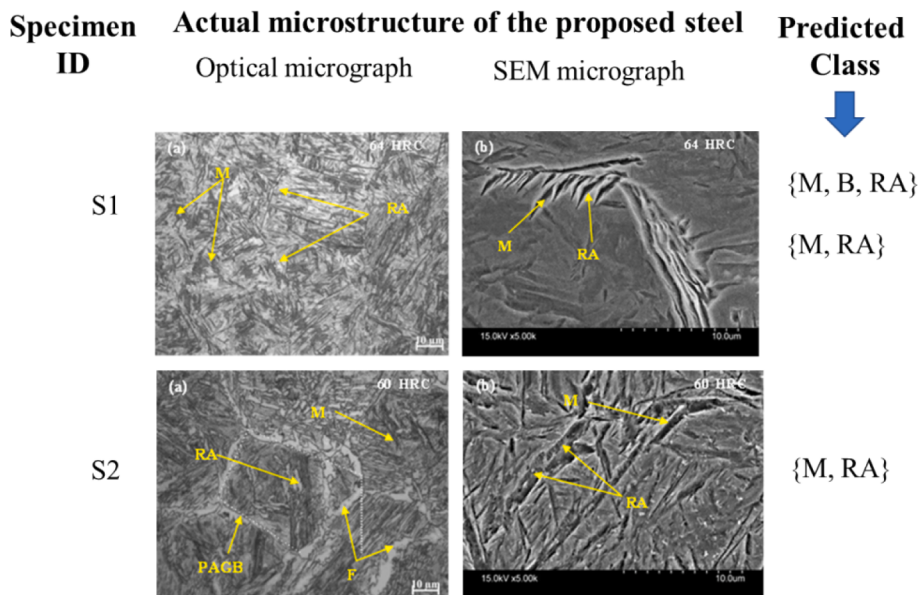


Fig. 13. Optical and SEM microstructures of the Q&P heat-treated steels correspond to the parameters set as reported in Table 5, depicting the efficacy prediction in re-engineering the composition and heat treatment parameter for a target microstructure type {M, RA}.

SEM image. There is also a fall in the hardness from 64 HRC to 60 HRC. This can be attributed to the formation of ferrite and retained austenite. It is clearly shown that the samples subjected to Q&P treatment have an almost similar microstructure. It is noteworthy that carbon transports from supersaturated martensite into the surrounding austenite during the partitioning step in the Q&P process, and thereby more austenite is retained down to room temperature [33]. Eventually, the multiphase microstructure of martensite, ferrite with retained austenite {M, F, RA} results in this case, which is a significant deviation against the model prediction of {M, RA} microstructure type. It can be recalled that the precision for {M, RA} type microstructure as appeared is poor (0.47), and class is a most confusing microstructure type to predict. This prediction is associated with relatively high uncertainty. A similar result has been depicted in experimentation also. Therefore, the recall and precision that is a type I and type II error is significant in the case of {M, RA} microstructure class, as evident from the model and the experimental results.

6. Conclusions

The study proposed a *k*-NN classifier for predicting Q&P steel microstructure types such as martensite-retained austenite {M, RA}, martensite-bainite-retained austenite {M, B, RA} etc. The proposed model has unfolded the effects of metallurgical features such as steel composition and Q&P heat treatment temperature on the evolution of the microstructure of this steel. Mn (wt.%) appears to be most important in the competitive evolution of martensite and retained austenite. The partitioning of Mn plays an important role in stabilization and thus promoting or restricting the martensite formation along with the M_s, QT and PT. Moreover, from the model insight study, it can be claimed that the model captures the physical metallurgical knowledge of the Q&P

steel and can be utilized to predict microstructure before synthesis. The following are the key conclusive outcome of the work:

- The *k*-NN classifiers trained with the pre-processed Q&P steel data could achieve the overall f1-score of 97.7% and 77.7 % in the training and testing dataset, respectively. Also, the prediction performance metrics for individual microstructure types are observed to be reasonably good ($\geq 77\%$) except for the martensite-retained austenite {M, RA} type microstructure. A high degree of uncertainty is observed in the prediction of {M, RA} type microstructure, and a relatively less 51% of f1-score is recorded in this case in the test data.
- The model study revealed that Mn %wt. and quenching and partitioning temperatures are the most important features in determining the type of microstructure of the Q&P steel.
- The re-engineering of the compositional and heat treatment parameter using the proposed classifier prediction could successfully identify a parameter window and associated real investigation microstructure depicted a similar 50% validation scenario of the model prediction for martensite-retained austenite {M, RA} microstructure type.

7. Data availability statement

The basic data and python code used in this research available as [supplementary materials](#). Also, can be found in Mendeley Data, V1, the reserved <https://doi.org/10.17632/g7kcvf98b.1>. For any other data reported in this manuscript will be made available on request.

CRediT authorship contribution statement

Ashutosh Kumar Gupta: Software, Formal analysis, Data curation, Methodology, Visualization, Writing – original draft. **Sunny Chakraborty:** Data curation, Investigation, Writing – original draft, Formal analysis. **Swarup Kumar Ghosh:** Investigation, Supervision, Validation. **Subhas Ganguly:** Conceptualization, Methodology, Supervision, Resources, Writing – review & editing, Project administration, Funding acquisition.

Declaration of Competing Interest

The authors declare that they have no known competing financial interests or personal relationships that could have appeared to influence the work reported in this paper.

Acknowledgement

This work is financially supported by the Science and Engineering Research Board, Department of Science and Technology (DST-SERB), India, under its Core Research Grant (CRG) scheme [Grant number: CRG/2021/005256].

Appendix A. Supplementary data

Supplementary data to this article can be found online at <https://doi.org/10.1016/j.commatsci.2023.112321>.

References

- [1] S. Gupta, A. Banerjee, J. Sarkar, M. Kundu, S.K. Sinha, N.R. Bandyopadhyay, S. Ganguly, Modelling the steel microstructure knowledge for in-silico recognition of phases using machine learning, *Mater. Chem. Phys.* 252 (2020), 123286, <https://doi.org/10.1016/j.matchemphys.2020.123286>.
- [2] B. Ma, J. He, A. Ramazani, N. Fehlemann, X. Wang, S. Münstermann, Irregular microstructure-property linkage for cast alloys by a novel deep learning approach: Application on cast austenitic stainless steel, *Mater. Today Commun.* 35 (2023), 105979, <https://doi.org/10.1016/j.mtcomm.2023.105979>.
- [3] Z. Yang, Y. Li, X. Wei, X. Wang, C. Wang, Martensite Start Temperature Prediction through a Deep Learning Strategy Using Both Microstructure Images and Composition Data, *Materials (Basel)* 16 (2023), <https://doi.org/10.3390/ma16030932>.
- [4] B.L. Decost, E.A. Holm, A computer vision approach for automated analysis and classification of microstructural image data, *Comput. Mater. Sci.* 110 (2015) 126–133, <https://doi.org/10.1016/j.commatsci.2015.08.011>.
- [5] T.D. Sparks, S.K. Kauwe, M.E. Parry, A.M. Tehrani, J. Brigoch, Machine Learning for Structural Materials, *Annu. Rev. Mater. Res.* 50 (2020) 27–48, <https://doi.org/10.1146/annurev-matsci-110519-094700>.
- [6] S.G. Baird, M. Liu, H.M. Sayeed, T.D. Sparks, Data-driven materials discovery and synthesis using machine learning methods, in: *Compr. Inorg. Chem.*, III, Elsevier, 2023, pp. 3–23, <https://doi.org/10.1016/B978-0-12-823144-9.00079-0>.
- [7] G. Lambard, K. Yamazaki, M. Demura, Generation of highly realistic microstructural images of alloys from limited data with a style-based generative adversarial network, *Sci. Rep.* 13 (2023) 1–13, <https://doi.org/10.1038/s41598-023-27574-8>.
- [8] L. Zhu, X. Yu, W. Li, L. Zhang, N. Zhang, Y. Lv, L. Zhao, W. Zhang, Z. Wang, H. Yu, Z. Bi, H. Han, J. Ruan, L. Jiang, High-throughput investigation of Nb and Ta alloying effects on the microstructure and properties of a novel Ni-Co-based superalloy, *Scr. Mater.* 226 (2023), 115215, <https://doi.org/10.1016/j.scriptamat.2022.115215>.
- [9] A. Chowdhury, E. Kautz, B. Yener, D. Lewis, Image driven machine learning methods for microstructure recognition, *Comput. Mater. Sci.* 123 (2016) 176–187, <https://doi.org/10.1016/j.commatsci.2016.05.034>.
- [10] J. Gola, D. Britz, T. Staudt, M. Winter, A.S. Schneider, M. Ludovici, F. Mücklich, Advanced microstructure classification by data mining methods, *Comput. Mater. Sci.* 148 (2018) 324–335, <https://doi.org/10.1016/j.commatsci.2018.03.004>.
- [11] G. Thewlis, Materials perspective: Classification and quantification of microstructures in steels, *Mater. Sci. Technol.* 20 (2004) 143–160, <https://doi.org/10.1179/026708304225010325>.
- [12] S.M. Azimi, D. Britz, M. Engstler, M. Fritz, F. Mücklich, Advanced steel microstructural classification by deep learning methods, *Sci. Rep.* 8 (2018) 1–14, <https://doi.org/10.1038/s41598-018-20037-5>.
- [13] C. Shen, C. Wang, M. Huang, N. Xu, S. van der Zwaag, W. Xu, A generic high-throughput microstructure classification and quantification method for regular SEM images of complex steel microstructures combining EBSD labeling and deep learning, *J. Mater. Sci. Technol.* 93 (2021) 191–204, <https://doi.org/10.1016/j.jmst.2021.04.009>.
- [14] S. Arivazhagan, J.J. Tracia, N. Selvakumar, Classification of steel microstructures using Modified Alternate Local Ternary Pattern, *Mater. Res. Express.* 6 (2019), <https://doi.org/10.1088/2053-1591/ab2d83>.
- [15] H. Kim, Y. Arisato, J. Inoue, Unsupervised segmentation of microstructural images of steel using data mining methods, *Comput. Mater. Sci.* 201 (2022), 110855, <https://doi.org/10.1016/j.commatsci.2021.110855>.
- [16] D. Bhattacharya, Metallurgical Perspectives on Advanced Sheet Steels for Automotive Applications, *Adv. Steels* (2011) 163–175, https://doi.org/10.1007/978-3-642-17665-4_18.
- [17] D.K. Matlock, J.G. Speer, E. De Moor, P.J. Gibbs, Recent Developments in Advanced High Strength Sheet Steels for Automotive Applications: An Overview, *JESTECH* 15 (2012) 1–12.
- [18] J. Sun, H. Yu, Microstructure development and mechanical properties of quenching and partitioning (Q&P) steel and an incorporation of hot-dipping galvanization during Q&P process, *Mater. Sci. Eng. A* 586 (2013) 100–107, <https://doi.org/10.1016/j.msea.2013.08.021>.
- [19] B.L. DeCost, T. Francis, E.A. Holm, Exploring the microstructure manifold: Image texture representations applied to ultrahigh carbon steel microstructures, *Acta Mater.* 133 (2017) 30–40, <https://doi.org/10.1016/j.actamat.2017.05.014>.
- [20] T. Dutta, D. Das, S. Banerjee, S.K. Saha, S. Datta, An automated morphological classification of ferrite-martensite dual-phase microstructures, *Meas. J. Int. Meas. Confed.* 137 (2019) 595–603, <https://doi.org/10.1016/j.measurement.2018.12.106>.
- [21] D. Fredriksson, Machine Learning Methods for Segmentation of Complex Metal Microstructure Features, 2022. <http://kth.diva-portal.org/smash/get/diva2:1679770/FULLTEXT01.pdf>.
- [22] S.W. Kim, S.H. Kang, S.J. Kim, S. Lee, Estimating the phase volume fraction of multi-phase steel via unsupervised deep learning, *Sci. Rep.* 11 (2021) 1–14, <https://doi.org/10.1038/s41598-021-85407-y>.
- [23] E.J. Seo, L. Cho, Y. Estrin, B.C. De Cooman, Microstructure-mechanical properties relationships for quenching and partitioning (Q&P) processed steel, *Acta Mater.* 113 (2016) 124–139, <https://doi.org/10.1016/j.actamat.2016.04.048>.
- [24] A. Arlazarov, O. Bouaziz, J.P. Masse, F. Kegel, Characterization and modeling of mechanical behavior of quenching and partitioning steels, *Mater. Sci. Eng. A* 620 (2015) 293–300, <https://doi.org/10.1016/j.msea.2014.10.034>.
- [25] N. Zhong, X.D. Wang, L. Wang, Y.H. Rong, Enhancement of the mechanical properties of a Nb-microalloyed advanced high-strength steel treated by quenching-partitioning-tempering process, *Mater. Sci. Eng. A* 506 (2009) 111–116, <https://doi.org/10.1016/j.msea.2008.11.014>.
- [26] C. hui Su, Q. guo Li, X. fei Huang, W. gang Huang, Effect of bainite microstructure during two-step quenching and partitioning process on strength and toughness properties of a 0.3%C bainitic steel, *J. Iron Steel Res. Int.* 25 (2018) 235–242, 10.1007/s42243-018-0032-4.
- [27] K. He, D. V. Edmonds, J.G. Speer, D.K. Matlock, F.C. Rizzo, EMC 2008 14th European Microscopy Congress 1–5 September 2008, Aachen, Germany, EMC 2008 14th Eur. Microsc. Congr. 1–5 Sept. 2008, Aachen, Ger. 2 (2008) 429–430, 10.1007/978-3-540-85226-1.
- [28] H. Guo, A. Zhao, R. Ding, C. Zhi, J. He, Quenching and partitioning steel produced through hot rolling, direct quenching and annealing, *Mater. Sci. Technol.* 32 (2016) 1605–1612, <https://doi.org/10.1080/02670836.2015.1133271>.
- [29] A. Gorni, Steel Forming and Heat-Treating Handbook, Internet Read Dec 20, 2022. (2015). www.gorni.eng.br.
- [30] U.S. Kevin Beyer, Jonathan Goldstein, Raghu Ramakrishnan, When is nearest neighbor meaningful?, 1999.
- [31] T. Cover, P. Hart, Nearest neighbor pattern classification, *IEEE Trans. Inf. Theory*. 13 (1967) 21–27, <https://doi.org/10.1109/TIT.1967.1053964>.
- [32] G. Mandal, S.K. Ghosh, S. Bera, S. Mukherjee, Effect of partial and full austenitisation on microstructure and mechanical properties of quenching and partitioning steel, *Mater. Sci. Eng. A* 676 (2016) 56–64, <https://doi.org/10.1016/j.msea.2016.08.094>.
- [33] K. Zhang, P. Liu, W. Li, F.C. Ma, Y.H. Rong, Quantitative Analysis of the Crystallographic Orientation Relationship Between the Martensite and Austenite in Quenching-Partitioning-Tempering Steels, *Acta Metall. Sin. (English Lett.)* 31 (2018) 659–667, <https://doi.org/10.1007/s40195-017-0683-3>.